Supplementary information for

Unconventional Fulde-Ferrell-Larkin-Ovchinnikov phase in a two-dimensional Ising superconductor

Puhua Wan[1], Oleksandr Zheliuk[1,2], Noah F. Q. Yuan[3], Xiaoli Peng[1], Le Zhang[1], Minpeng Liang[1], Uli Zeitler[2], Steffen Wiedmann[2], Nigel Hussey[2], Thomas T. M. Palstra[4], and Jianting Ye[1]

[1]Device Physics of Complex Materials, Zernike Institute for Advanced Materials, University of Groningen, 9747 AG Groningen, The Netherlands

[2]High Field Magnet Laboratory (HFML-EMFL), and Institute of Molecules and Materials, Radboud University, Toernooiveld 7, 6525 ED Nijmegen, Netherlands

[3]School of Science, Harbin Institute of Technology, Shenzhen 518055, China

[4] University of Twente, Drienerlolaan 5, 7522 NB Enschede, The Netherlands

1. **Mean-free path and clean superconductivity**
2. **Simulated effect of canting on 2D superconductors**
3. **The magnitude of six-fold anisotropy**
4. **In-plane isotropy of monolayer MoS_2**
5. **Excluding the two-gap scenario for the upturn in $B_{c2}(T)$**

1. Mean-free path and clean superconductivity

For semiconducting 2*H*-polytype transition metal dichalcogenides (TMDs such as the 2*H*-MoS_2 and WS_2,), the low-doping metallic state can have all carriers confined in a single band. Therefore, the 2D carrier density n_{2D} can be experimentally determined by measuring the Hall effect, where the n_{2D} is related to the Hall coefficient R_H as

$$n_{2D} = -\frac{1}{R_H e}. \quad \text{(S1)}$$

In contrast, the metallic 2*H*-$NbSe_2$ has a complex Fermi surface composed of five pockets, having both hole and electron-like carriers. From the zone center, hole-like carriers are found in multiple pockets including a small pancake-shaped pocket closed at Γ point as well as honeycomb-shaped and triangular-shaped cylindrical pockets centered at *K* and Γ points, respectively. Also, two electron-like pockets have honeycomb and triangular cylindrical shapes at *K* and Γ points, respectively[1]. The small pancake pocket at Γ point is either gapless or has a very small gap that is easily suppressed in a parallel external field due to its 3D Nature. It was reported that the small pancake pocket at Γ point is gapless even at a temperature much lower than T_{c0} (~ $0.003T_{c0}$) and gives rise to the quantum oscillations in the superconducting states[1,2]. The larger superconducting gaps open on the Fermi surface at the large hole-like pockets at *K* and Γ points, as shown in the ARPES measurements[2,3].

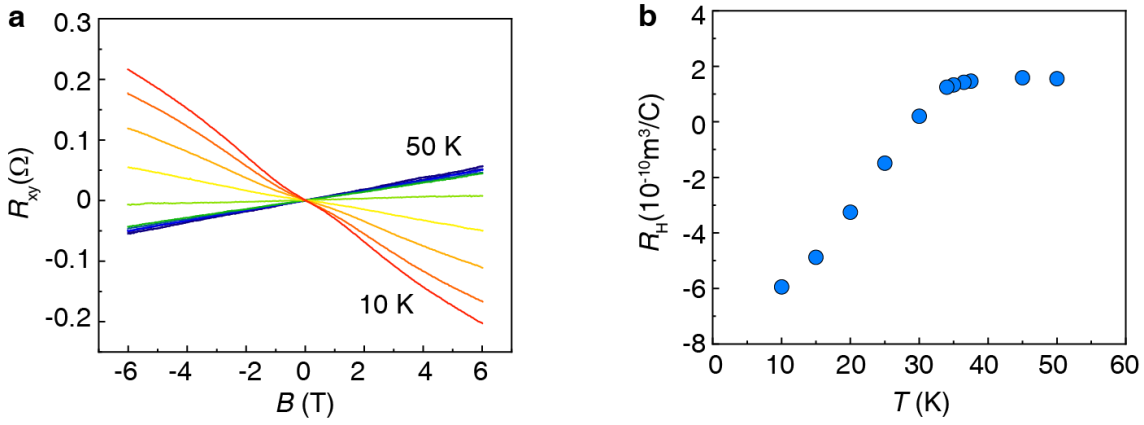

Figure S1 | Temperature dependence of Hall coefficient. a. Hall effect measurement at different temperatures. The transverse $R_{xy}(B)$ curve is shifted vertically at $B = 0$ to null the small pickup from the longitudinal R_{xx} channel. **b.** The Hall coefficient as a function of temperature.

Having carriers from two Fermi pockets, say contributed by both electrons and holes with carrier density n and p, then the R_H is

$$R_H = \frac{nu_n^2 - pu_p^2}{e(nu_n + pu_p)^2}, \quad \text{(S2)}$$

where u_n and u_p the electron and hole mobilities, respectively. As shown in Fig. S1a, the R_H of $NbSe_2$ flake changes the sign showing a switch from the hole- to electron-like transport at $T \sim T_{CDW}$, which is consistent with Ref. 4 of this supplementary information. In the low B field, Ong[5] shows that the Hall transport of mixed carriers can be described as

$$R_H = \frac{2\pi d(l_p^2 - l_n^2)}{e\left[(k_{F,p}l_p)^2 + (k_{F,n}l_n)^2\right]}. \quad \text{(S3)}$$

The l_n, l_p and the $k_{F,n}$, $k_{F,p}$ are the mean free paths and the wave vectors of holes and electrons, respectively. Due to the dramatic increase of electron mean-free path, the R_H changes the sign below T_{CDW}. Since the electrons are the minority above T_{CDW}, we can assume there is a single type of carrier and use the R_H measured at T = 40 K > T_{CDW} (as shown in Fig. S1b) to estimate the carrier density of holes using Eq. S1. The estimated hole concentration is $p \approx 2.4 \times 10^{15}$ cm^{-2} for a single layer, which is larger than the results from band structure calculation[4] $p = 8.51 \times 10^{14}$ cm^{-2}. Using this larger p, we can estimate the lower limit of the mean-free-path using the 2D Drude's formula,

$$l_{2D} = \frac{h}{e^2}\frac{\sigma_{2D}}{\sqrt{2\pi p}}, \quad \text{(S4)}$$

where $\sigma_{2D} = \frac{1}{NR_s}$ is the conductance of a single layer, where N is the total layer number. From the sheet resistance R_s measured right above T_c, we can determine the mean-free-path $l_{2D} \approx 30$ nm. The zero temperature Ginzburg-Landau (GL) coherence length ξ can be extracted from the temperature dependence of the upper critical field $B_{c2,\perp}$ in the perpendicular magnetic fields

$$B_{c2,\perp} = \frac{\Phi_0}{2\pi\xi(0)^2\left(1 - \left(\frac{T}{T_c}\right)\right)}, \quad \text{(S5)}$$

where Φ_0 is the flux quantum. At T = 0 K, the GL $\xi(0)$ = 8.3 nm. From the GL ξ, we can obtain the Pippard coherence length of a clean superconductor $\xi_0 = 1.35\xi(0)$ = 11.2 nm[6]. Satisfying $\xi_0 < l_{2D}$ brings our system into the clean limit.

As shown in Eq. S5, for a multi-gap superconductor, a smaller gap, with a smaller $B_{c2,\perp}$, has a larger ξ_0. Therefore, the larger ξ_0, associated with the smaller gaps, may violate the clean-limit criteria $\xi_0 < l_{2D}$. On the other hand, the smaller gaps are also easier to be suppressed by the external *B* fields. Hence, in high fields where the orbital FFLO phase appears, the larger gaps, surviving at $B > B^*$, ensure a clean superconductivity in the orbital FFLO regime.

2. Simulated effect of canting on 2D superconductors

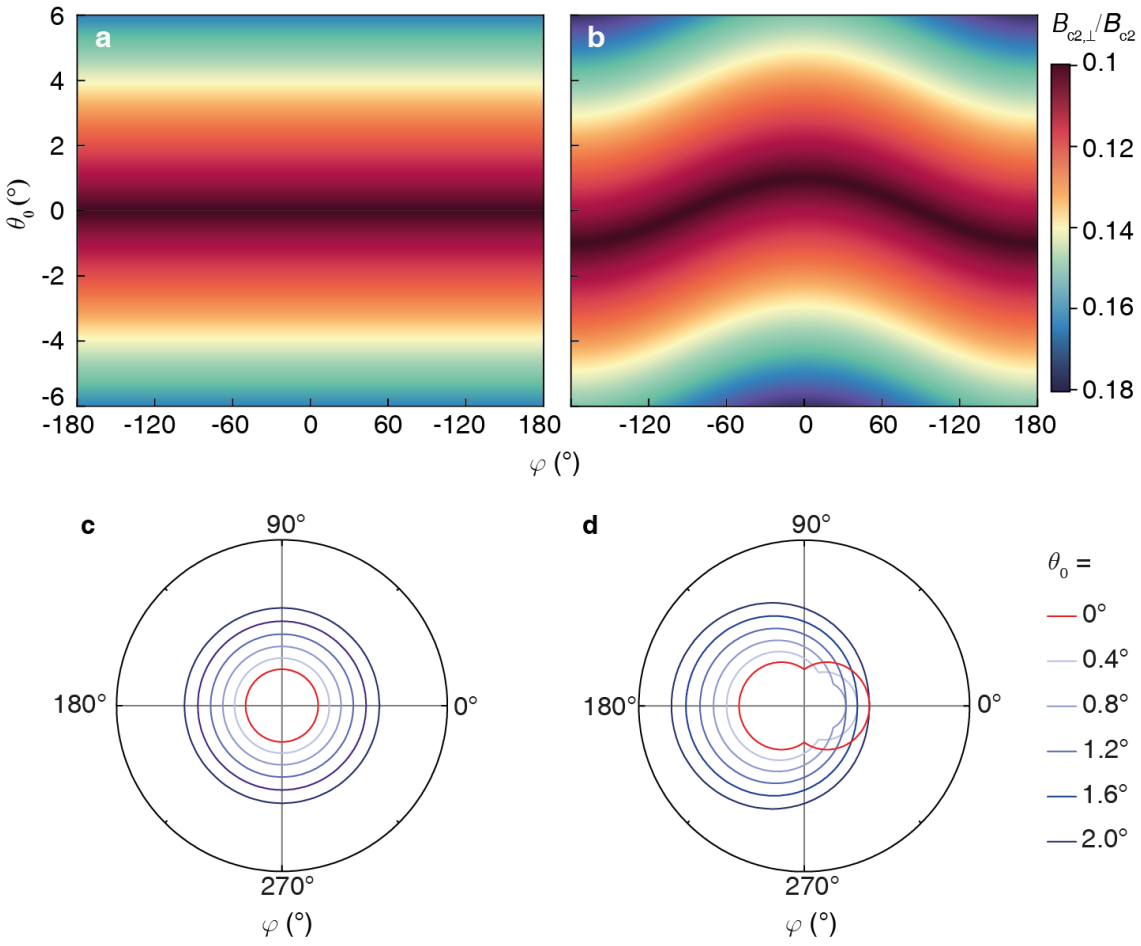

Figure S2 | Simulated effect of canting on an isotropic 2D superconductor. We simulate a superconductor with an anisotropy $B_{c2}^{\parallel}/B_{c2}^{\perp} = 10$, which is typically found in Ising superconductors. The canting angle is set as **a.** $\gamma = 0°$ and **b.** $\gamma = 1°$. The polar plots of $B_{c2}^{\perp}/B_{c2}$ show **c.** isotropic for $\gamma = 0°$, whereas shows **d.** a fake two-fold anisotropy when $\gamma \neq 0$.

It is worth emphasizing that having the γ can pick up the effect of misaligned B fields, leading to wrong conclusions for the anisotropy of superconductivity at in-plane B fields. In Fig. S2 we show the simulated $B_{c2}(\varphi, \theta_0)$ of isotropic 2D superconductivity combining Eq. 4 and Eq. 5 in the Methods. The out-of-plane anisotropy is set as $B_{c2}^{\parallel}/B_{c2}^{\perp} = 10$, mimicking a typical Ising superconductor with large anisotropy. When the effect of γ is ignored (in this case, θ_0 is a constant), the $B_{c2}(\varphi)$ oscillates as a function of φ, exhibiting a two-fold symmetry as shown in Fig. S2d. This erroneous two-fold anisotropy originates from picking up the $B_{\perp}$ components due to the cantering.

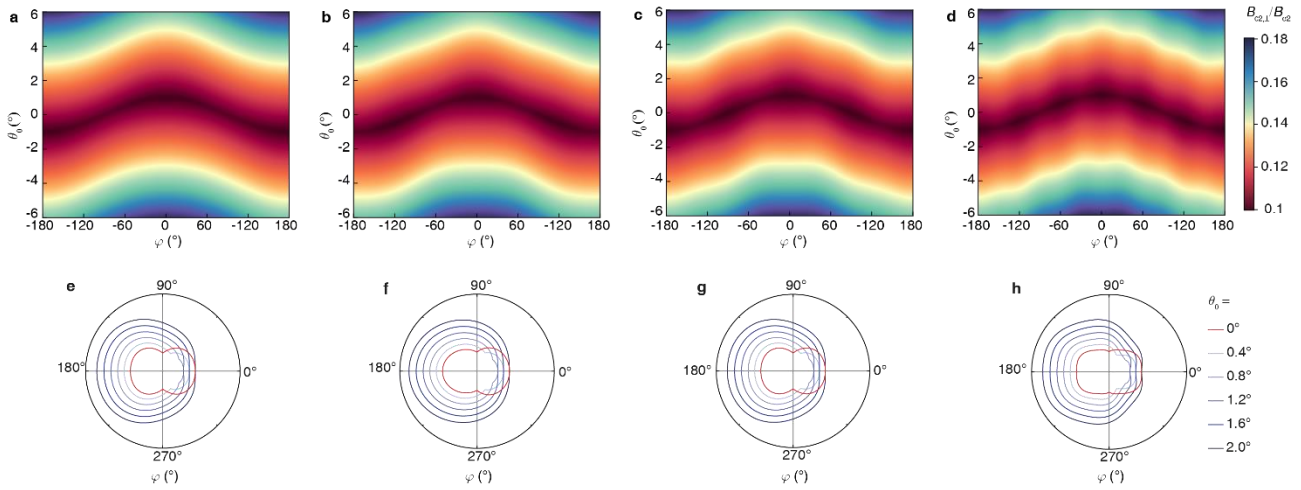

Figure S3 | Simulated effects of having a canting angle in measuring 2D superconductors with intrinsic in-plane anisotropies. We set the out-of-plane anisotropy $B_{c2}^{\parallel}/B_{c2}^{\perp}$ = 10 and the canting angle γ = 1°. The intrinsic in-plane anisotropy of the 2D superconductor is simulated as $B_{c2}(\varphi, \theta = 0) = a + bcos(\frac{n\pi\varphi}{180})$ with *n* denoting the folds of the intrinsic anisotropy. The amplitude of in-plane anisotropy is $\frac{B_{c2,\parallel}^{max} - B_{c2,\parallel}^{min}}{B_{c2,\parallel}^{max}} = \frac{2b}{a+b}$ = 0.02. The effect of cantering on $B_{c2}(\varphi)$ is plotted as mapping for **a.** two-, **b.** three-, **c.** four-, and **d.** six-fold intrinsic anisotropies. **e - h.** The corresponding polar plots all show erroneous two-fold anisotropies.

Furthermore, we simulate how the presence of γ can obscure the intrinsic anisotropy. We first introduce an intrinsic anisotropy, manifested in the upper critical field as $B_{c2}(\varphi, \theta = 0) = a + bcos(\frac{n\pi\varphi}{180})$, where *n* denotes the number of folds of the anisotropy. We assume the amplitude of in-plane anisotropy $\frac{B_{c2,\parallel}^{max} - B_{c2,\parallel}^{min}}{B_{c2,\parallel}^{max}} = \frac{2b}{a+b}$ = 0.02 which is close to our present measurement. In the presence of γ, the $B_{\perp}$ component can show a two-fold anisotropy, hence inducing "fake" two-fold anisotropies in $B_{c2}(\varphi)$. Due to the direct orbital contribution from the two-fold $B_{\perp}$, the contribution is much stronger than the intrinsic three-, four-, or six-fold anisotropy (Fig. S3e-h). Therefore, eliminating the influence of the canting angle γ is an essential step for the accurate determination of intrinsic in-plane anisotropies, which is indispensable for 2D superconductors with strong anisotropies.

3. The magnitude of six-fold anisotropy

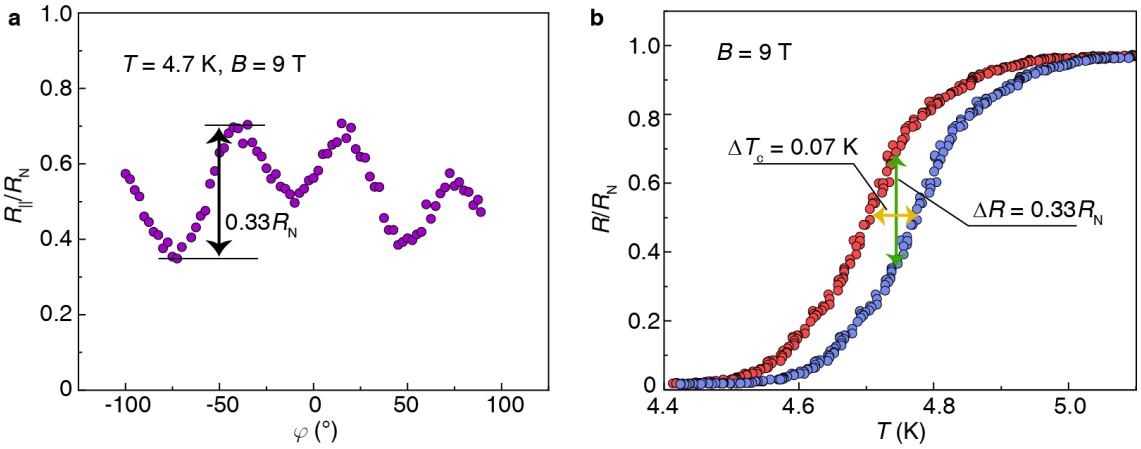

Figure S4 | Evaluating the amplitude of the six-fold anisotropy at B = 9 T. a. From the same data shown in Main Text Fig. 3c at T = 4.7 K and B = 9 T (main text), the resistance oscillates as a function of φ, due to the change of T_c at different φ angles. The amplitude is determined as $R_{\parallel,max} - R_{\parallel,min} = 0.33R_N$ **b.** The superconducting transition at B = 9 T (red dots) is shifted horizontally by ΔT_c = 0.07 K. The amplitude of six-fold anisotropy is quantified as $4k_B\Delta T_c$ = 0.02 meV. Here, the coefficient 4 was used in the analysis of the largest gap at the K pockets reported in ARPES measurements[7].

Although the accuracy of the angle sensor of our rotation stage is better than 0.1°, it still limits the precision in aligning the B field parallel to the 2D sample surface. We assume a limiting case in which the maximum angular error is doubled to 0.2° when we compare the T_c values at two different φ values. As shown in Fig. 2b in the main text, the deviation of 0.2° leads to an error of 0.2 T in B_{c2} when θ is close to 0°. The angular accuracy limits the determination of exact energy scales by measuring the B_{c2} as a function of φ.

On the other hand, as shown in Main Text Fig. 3c, the amplitude of the six-fold anisotropy grows with the increase of B field after entering the orbital FFLO phase. At a given temperature and magnetic field along the FFLO phase boundary, a state with smaller resistance corresponds to a higher T_c. Therefore, we can quantify the in-plane anisotropy of T_c by measuring the azimuthal φ dependence of $R(\varphi, \theta = 0)$. At $B_\parallel$ = 9 T, we find the $R_{\parallel,max} - R_{\parallel, min} = 0.33R_N$.

For the maximum change of $0.33R_N$ caused by the azimuthal rotation, we can then determine the corresponding change of ΔT_c from the R(T) dependences. As shown in Fig. S4a, the $R_{\parallel, max}$ and $R_{\parallel, min}$ appears at $0.7R_N$ and $0.37R_N$, respectively. Therefore, we shift the $R(T)$ dependence measured at $B_\parallel$ = 9

T to $R(T + \Delta T_c)$. As shown in Fig. S4b, the shift ensures that $\Delta R = 033R_N$ for the minimum T_c appears at ~$0.7R_N$ and maximum T_c at ~$0.4R_N$, respectively. The corresponding ΔT_c is then determined as 0.07 K.

The amplitude of gap anisotropy is quantified as $xk_B\Delta T_c$, where k_B is the Boltzmann constant. As indicated by the ARPES measurement[7], the coefficient x is 4 for the larger superconducting gap at the *K* pockets and 1.76 for the smaller one at Γ pockets. Here, we choose the largest gap at the *K* pockets, which have a medium coupling strength (*9)* and remains open at B = 9 T. Hence the ΔT_c = 0.07 K yields an anisotropy of $4k_BT_c$ = 0.02 meV in the orbital FFLO state, which is about 0.8% of the largest superconducting gap at the *K* pocket (2.5 meV).

4. In-plane isotropy of monolayer MoS_2

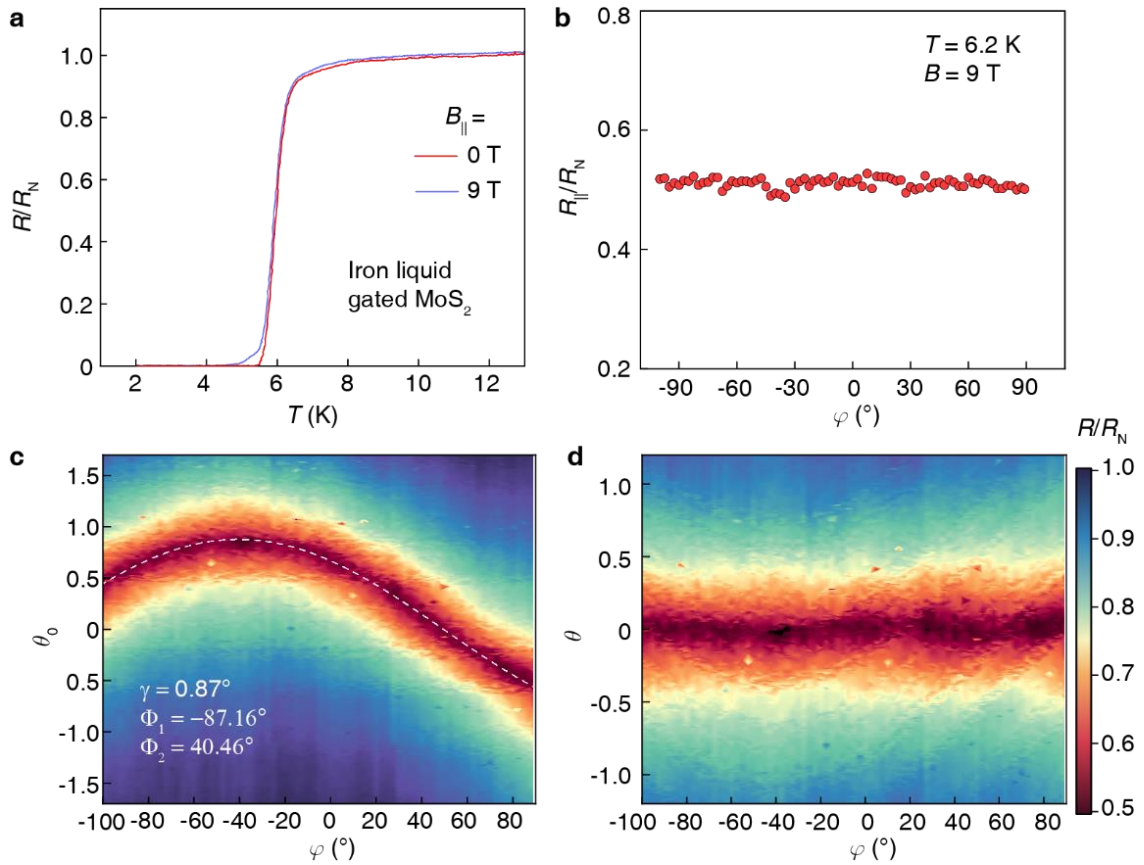

Figure S5 | In-plane isotropy of ion-gated monolayer superconductivity in a multilayer MoS_2. a. Superconducting transition in in-plane field B = 0 and 9 T. **b.** Magnetoresistance $R_{\|}(\varphi)$ remains constant at different φ showing isotropic response. **c.** Mapping of $R(\theta_0, \varphi)$ before subtracting the effect of canting angle. The white dashed line is a fit using Eq. 5 in the Methods, which yields a canting angle $\gamma = 0.87°$. **d.** Mapping of $R(\theta, \varphi)$ after subtracting the effect of canting angle.

The 2*H*-type MoS_2 and $NbSe_2$ are identical in the crystal structure, except for a shift of transition metal position, which is further divided as $2H_a$ and $2H_b$ types. Since Mo has one more valence electron than Nb, the 2*H*-MoS_2 has a fully filled band. By chemical intercalation or electrostatic gating, the semiconducting MoS_2 can be doped into metallic states, where superconductivity is realized at a carrier density $n_{2D} > 8\times10^{13}$ cm^{-2}. The ion-gated few-layer MoS_2 is superconducting only in the top first layer due to the strong screening effect of the electric field[8]. Like a $NbSe_2$ monolayer, the broken inversion symmetry induces the Ising SOC, which locks the electron spins to the out-of-plane direction, strongly protecting the Cooper pairs against an in-plane field $B_{\|}$. Therefore, the $B_{c2,\|}$ can go well beyond the Pauli limit B_p, reaching ~ $6B_p$[8].

Comparing the superconductivity in a multilayer $NbSe_2$ and a confined monolayer MoS_2 can highlight the contribution of current-driven vortex motion in the out-of-plane direction, which only exists in a multilayer. We perform the exact measurement to study the anisotropy of superconducting MoS_2 (T_c = 6 K) in a parallel B field. As shown in Fig. S5, after subtracting the contribution of the canting angle (γ = 0.87°), the superconductivity is highly isotropic. Therefore, the two-fold anisotropy induced by the Lorentz force is not observed in this control experiment as the interlayer motion is completely suppressed in a monolayer superconductor.

The absence of two-fold anisotropy confirms that the ionic gating induces superconductivity in the outer first layer. More importantly, since monolayer thickness prohibits any interlayer interaction, this also suppresses the FFLO state since the orbital FFLO phase observed in multilayer $NbSe_2$ requires an interlayer orbital effect between two Ising superconducting layers with inversion symmetry. Hence, the six-fold anisotropy associated with the orbital FFLO phase is also absent in the ion-gated MoS_2.

5. Excluding the two-gap scenario for the upturn in B_{c2} (T)

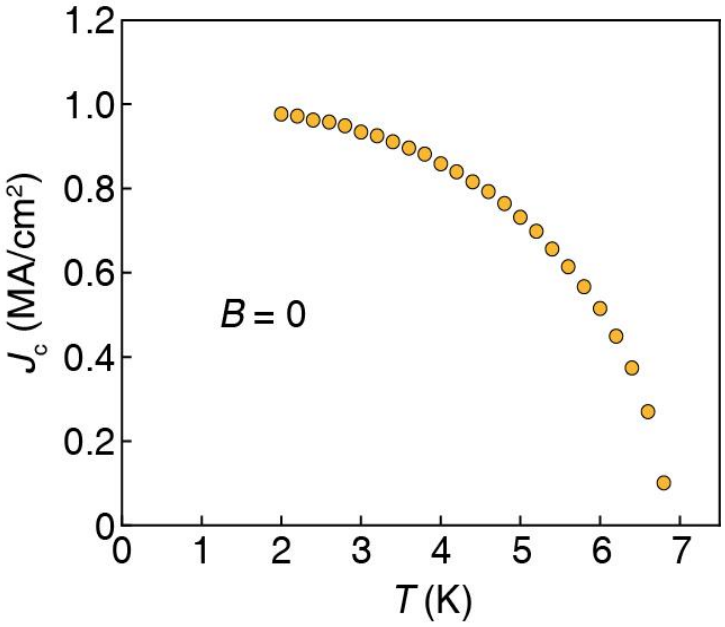

Figure S6 | Critical current density as a function of temperature under a zero magnetic field. At B = 0 T, no upturn was observed in the temperature dependence of J_c. This rules out the two-gap scenario as the cause of the upturns.

The superconducting gaps of $NbSe_2$ open at both K and Γ points for both hole- and electron-like pockets as shown in the ARPES results[7,9]. The multiple gaps of different gap size may lead to kinks in both $B_{c2}(T)$[10] and $J_c(T)$[11]. On the other hand, in dirty two-gap superconductors, the upturn in $B_{c2}(T)$ is also expected due to interband scattering[10].

First of all, we can rule out the possibility of having the dirty two-gap scenario since our device shows superconductivity in the clean regime. Furthermore, the kink observed in $|\theta| < 1°$, as shown in the $B_{c2}(\theta)$ in Main Text Fig. 2b, can not be described by the dirty two-gap model[10]. Second, the two-gap scenario would expect the temperature dependence of J_c to show a kink when the second gap opens at $T < T_{c0}$ under the zero B field[11]. As shown in Fig. S6, the $J_c(T)$ measured at B = 0 T has a smooth dependence without showing kink as a function of temperature. Instead, the kinks in J_c appear when the B field is applied crossing the uniform superconductor/orbital FFLO phase boundary as shown in Main Text Fig. 4a. The phase boundary thus determined by $J_c(B)$ agrees well with the tricritical point that is determined by $B_{c2}(T)$ measurements. Hence, we can also safely rule out the two-gap scenario as the cause of the kinks observed in our devices.

References

1. Corcoran, R. *et al.* Quantum oscillations in the mixed state of the type II superconductor 2H-$NbSe_2$. *J. Phys. Condens. Matter* **6**, 4479 (1994).
2. Yokoya, T. Fermi Surface Sheet-Dependent Superconductivity in 2H-$NbSe_2$. *Science* **294**, 2518–2520 (2001).
3. Rossnagel, K. *et al.* Fermi surface of 2H-$NbSe_2$ and its implications on the charge-density-wave mechanism. *Phys. Rev. B* **64**, 1–6 (2001).
4. Bel, R., Behnia, K. & Berger, H. Ambipolar Nernst Effect in $NbSe_2$. *Phys. Rev. Lett.* **91**, 2–5 (2003).
5. Ong, N. P. Geometric interpretation of the weak-field Hall conductivity in two-dimensional metals with arbitrary Fermi surface. *Phys. Rev. B* **43**, 193–201 (1991).
6. Tinkham, M. *Introduction to Superconductivity 2nd*. (Dover, 1996).
7. Rahn, D. J. *et al.* Gaps and kinks in the electronic structure of the superconductor 2H-$NbSe_2$ from angle-resolved photoemission at 1 K. *Phys. Rev. B* **85**, 1–8 (2012).
8. Lu, J. M. *et al.* Evidence for two-dimensional Ising superconductivity in gated MoS_2. *Science* **350**, 1353–1357 (2015).
9. Kiss, T. *et al.* Charge-order-maximized momentum-dependent superconductivity. *Nat. Phys.* **3**, 720–725 (2007).
10. Gurevich, A. Enhancement of the upper critical field by nonmagnetic impurities in dirty two-gap superconductors. *Phys. Rev. B* **67**, 184515 (2003).
11. Talantsev, E. F. *et al.* On the origin of critical temperature enhancement in atomically thin superconductors. *2D Mater.* **4**, 025072 (2017).